J. King Saud Univ., Vol. 11, *Eng. Sci.* (1), pp. 117-130 (A.H. 1419/1999)

Reattachment of Turbulent Shear Layer over a Backward Facing Step with Isotropic Porous Floor Segments

Bassam A.K Abu-Hijleh
Mechanical Engineering Department, Jordan University of Science & Technology (JUST)
P.O.Box 3030, Irbid 22110, Jordan

(Received 24 September 1997; accepted for publication 16 February 1998)

Abstract. The incompressible turbulent reattaching flow over a 2-D backward facing step with different length porous floor segments was solved numerically using the finite element numerical method. The accuracy of the numerical solution was established by comparing the numerical results to experimental measurements reported in the literature. Three different floor configurations with different normalized length isotropic porous segments, X_p = 4, 8, and 12, were studied. The porosity of each segment was varied over a wide range by changing the value of the pressure loss coefficient (KP). The variation of the normalized reattachment length (X_r), normalized maximum recirculation velocity (U_{rec}), and normalized maximum turbulent kinetic energy (TKE) are reported and discussed for all configurations. The results show that, depending on the length and loss coefficient of the segments, a floor with porous segments can significantly change the values of X_r, U_{rec}, and TKE.

Nomenclature

C_0	Constant used in Eq. (7)
C_1	Variable used in Eqs. (5) and (6)
C_2	Variable used in Eqs. (5) and (6)
C_μ	Constant used in Eq.(4)
G	Variable used in Eq. (8)
H	Step height
K	Turbulent kinetic energy ($u^2 + v^2$)
KP	Pressure loss coefficient in porous region
P	Pressure

TKE	Normalized maximum turbulent kinetic energy, K_{max}/U_∞^2
U	Time-averaged axial velocity
U_∞	Incoming free stream axial velocity
U_{rec}	Maximum axial recirculation velocity
u	Axial velocity fluctuation
V	Time-averaged transverse velocity
v	Transverse velocity fluctuation
X	Axial distance normalized by step height, x/H
X_r	Normalized reattachment length
X_p	Normalized length of porous segment
x	Axial distance measured from the step corner
y	Vertical distance measured from the step corner

Greek letters

β	Constant used in Eq. (7)
ε	Turbulent energy dissipation
η	Variable used in Eq. (7)
η_0	Constant used in Eq. (7)
μ	Viscosity
μ_t	Eddy viscosity
ρ	Density
σ_K	Constant used in Eq. (5)
σ_ε	Constant used in Eq. (6)

Introduction

The flow over a backward facing step has been studied extensively. This flow is used to simulate a wide range of flow fields both external, e.g., the base flow over a rocket, and internal, e.g., combustion chamber. The enhancement or reduction, depending on the application of the flow reattachment location, recirculation flow velocity and turbulence is

desirable. This idea has received a lot of attention in the literature. The control mechanism can be either active or passive. Recent work in the area of active control has focused of the use of acoustic excitation [1], mass injection or bleeding [2], vortex generators [3], imposed wall heat flux [4], and moving fences or flaps [5]. Passive control methods incorporate fixed attachments in order to modify the flow for a given range of operating conditions. Such methods include the use of surface riblets [6], properly sized cavities [7], and porous surfaces [8]. A more comprehensive review of earlier work in the area of boundary layer control can be found in Gad-el-Hak and Bushnell [9]. The attraction of passive methods is their relative ease of use in practical situations. The main drawback is the limited range of operating conditions under which such arrangements are effective.

The current work focuses on the effect of the porosity of different floor segments on the flow reattachment location, recirculation flow velocity, and turbulence of a 2-D incompressible turbulent boundary layer flow over a backward facing step. This model could serve as a passive control mechanism. More importantly, this model could be used to study the effect of solid fuel packing in a solid fuel combustion chamber. The small passages between the solid fuel particles could be modeled as a porous segment in the combustion chamber. The effect of floor segment porosity was studied numerically for three different porous floor segments. The numerical analysis is based on the Renormalized Group Theory (RNG) two equation turbulence model. The equations were solved using a nonuniformly sized finite-element mesh. The numerical method was first validated against the experimental data of Kim *et al.* [10] for a fully turbulent incompressible boundary layer over a backward facing step. The Reynolds number based on inlet centerline velocity and momentum thickness at separation, $x = 0$, of the incoming boundary layer is 1.3×10^3. Figure 1 shows a schematic of the flow field under investigation including a generic porous segment.

Mathematical Model

The Reynolds averaged continuity, x-momentum, and y-momentum equations for steady flow, two-dimensional, incompressible, and constant properties fluid can be written as [11]:

$$\frac{\partial U}{\partial x} + \frac{\partial V}{\partial y} = 0 \tag{1}$$

$$\rho U\frac{\partial U}{\partial x} + \rho V\frac{\partial U}{\partial y} = -\frac{\partial P}{\partial x} - KP\frac{\rho U^2}{2} + \frac{\partial}{\partial x}\left[(\mu+\mu_t)\frac{\partial U}{\partial x}\right] + \frac{\partial}{\partial y}\left[(\mu+\mu_t)\frac{\partial U}{\partial y}\right] \tag{2}$$

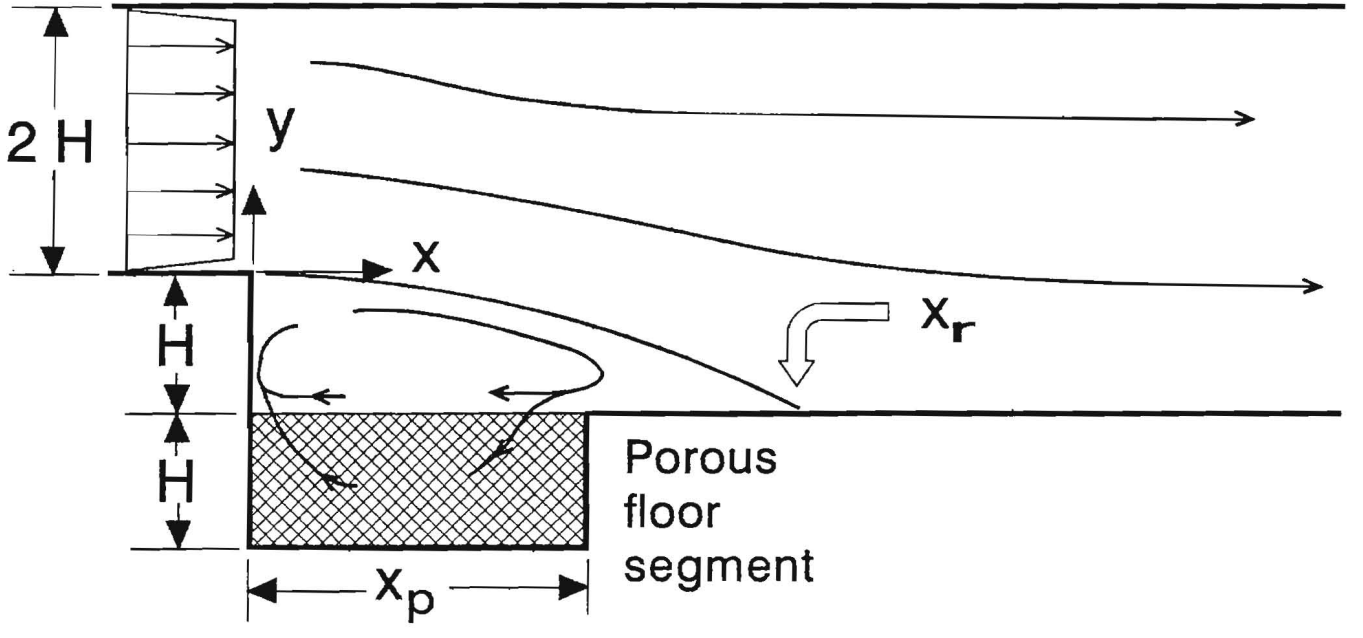

Fig. 1. Schematic of the flow field including a generic porous floor segment.

$$\rho U\frac{\partial V}{\partial x} + \rho V\frac{\partial V}{\partial y} = -\frac{\partial P}{\partial y} - KP\frac{\rho V^2}{2} + \frac{\partial}{\partial x}\left[(\mu+\mu_t)\frac{\partial V}{\partial x}\right]+\frac{\partial}{\partial y}\left[(\mu+\mu_t)\frac{\partial V}{\partial y}\right] \quad (3)$$

The second term on the right hand side of the momentum equations represents the extra pressure drop term due to the flow of the fluid through the passages of the porous segment. The pressure loss coefficient factor KP is used to relate the extra pressure drop to the local velocity. In the nonporous part of the flow, KP=0. The value of KP for different porous materials and arrangements can be found in fluid resistance books such as the Handbook of Hydraulic Resistance [12]. Note that the same constant KP is used in both momentum equations. This indicates an isotropic porous material, i.e. the pressure drop coefficient in both directions is the same. The effect of orthotropic porous material, i.e., $KP_x \neq KP_y$, is currently under investigation by the author. The turbulence effective eddy viscosity, μ_t, is given by:

$$\mu_t = C_\mu \rho\frac{K^2}{\varepsilon} \quad (4)$$

In Eq. (4), C_μ is a model constant. The turbulent kinetic energy, K, and the turbulent energy dissipation, ε, are governed by the following equations [11]:

$$\rho U\frac{\partial K}{\partial x}+\rho V\frac{\partial K}{\partial y}=\frac{\partial}{\partial x}\left[\left(\frac{\mu_t}{\sigma_K}+\mu\right)\frac{\partial K}{\partial x}\right]+\frac{\partial}{\partial y}\left[\left(\frac{\mu_t}{\sigma_K}+\mu\right)\frac{\partial K}{\partial y}\right]-\rho\varepsilon+$$

$$\mu_t\left[2\left(\frac{\partial U}{\partial x}\right)^2+2\left(\frac{\partial V}{\partial y}\right)^2+\left(\frac{\partial U}{\partial y}+\frac{\partial V}{\partial x}\right)^2\right] \quad (5)$$

$$\rho U\frac{\partial \varepsilon}{\partial x}+\rho V\frac{\partial \varepsilon}{\partial y}=\frac{\partial}{\partial x}\left[\left(\frac{\mu_t}{\sigma_\varepsilon}+\mu\right)\frac{\partial \varepsilon}{\partial x}\right]+\frac{\partial}{\partial y}\left[\left(\frac{\mu_t}{\sigma_\varepsilon}+\mu\right)\frac{\partial \varepsilon}{\partial y}\right]-C_2\rho\frac{\varepsilon^2}{K}+$$

$$C_1\mu_t\frac{\varepsilon}{K}\left[2\left(\frac{\partial U}{\partial x}\right)^2+2\left(\frac{\partial V}{\partial y}\right)^2+\left(\frac{\partial U}{\partial y}+\frac{\partial V}{\partial x}\right)^2\right] \quad (6)$$

In Eqs. (4-6), C_1, C_2, σ_K, and σ_ε are constants. Equations (4-6) constitute the standard K-ε model. This is an isotropic turbulence model and tends to underestimate the reattachment length for the flow under investigation [13]. Yakhot and Orszag [14] introduced a modified K-ε model based on the Renormalized Group Turbulence Theory (RNG). At high Reynolds numbers, the RNG has the same general form as the standard K-ε method but with different numerical values for the constants. The RNG method is intended

to give more accurate predictions in regions of low Reynolds numbers such as near the flow reattachment. In the RNG model, C_1 is a variable calculated from [11]:

$$C_1 = C_0 - \frac{\eta\left(1-\frac{\eta}{\eta_0}\right)}{1+\beta\eta^3} \tag{7}$$

where

$$\eta = \frac{\sqrt{G}\,K}{\varepsilon} \tag{8}$$

and

$$G = 2\left[\left(\frac{\partial U}{\partial x}\right)^2 + \left(\frac{\partial V}{\partial y}\right)^2\right] + \left(\frac{\partial U}{\partial y} + \frac{\partial V}{\partial x}\right)^2 \tag{9}$$

The value of the constants for the RNG model are [11]: $C_m = 0.085$, $C_0 = 1.42$, $C_2 = 1.68$, $\beta = 0.015$, $\eta_0 = 4.38$, and $\sigma_K = \sigma_\varepsilon = 0.7179$.

Validation of Numerical Code

The governing equations were solved by discretizing Eqs. (1-9) using a nonuniform quadrilateral element mesh. Smaller elements were located near the walls and in regions of high gradients, i.e., step corner and reattachment location. The mesh size was varied in order to obtain a mesh independent solution. The mesh used for the flow field, excluding the porous region, consisted of 6700 elements. When the reference flow field was solved using a mesh made of 11000 elements, the change in the reattachment length and TKE was less than 1%. Thus, the solution obtained using the 6700 element mesh was deemed to be mesh independent. Full mass balance between the inlet and exit planes was also achieved using the 6700 element mesh. This is another indication that this mesh is adequate for the flow field under investigation. The 6700 element mesh was used for all flow fields except for the long porous section case, $X_p = 12$. For $X_p = 12$, the downstream exit plane was extended by an additional ten step heights. This was necessary in order to give the flow field enough distance to reach uniform flow at the exit. This was the largest mesh used at 9000 elements, including the elements in the porous region. The addition of the porous segments required additional elements to mesh the porous region. The number of additional elements ranged form 780 to 2340 elements. Figure 2 shows the four mesh systems used in this work.

The discretized equations were solved iteratively using the streamline upwind method [15]. At the flow inlet plane, the velocity and turbulence kinetic energy conditions were specified as given by the experimental data of Kim *et al.* [10]. Only one boundary condition is required for the pressure. Since this is an incompressible flow, a reference value for the pressure is needed anywhere within the flow field. A zero gage pressure was specified at the exit plane. The axial gradients of the mean velocity, U, turbulent kinetic energy, K, and turbulent kinetic dissipation, ε, were set to zero at the exit plane. This served as the second axial boundary condition for the rest of the variables. No slip conditions at the walls were used for the transverse direction boundary conditions. The solution was deemed to have converged when the residual of each of U, V, P, K, and ε became less that 5×10^{-4}. The use of smaller tolerance values, 10^{-5} and 10^{-6}, resulted in all calculated values.

The first task was to check the ability of the code to predict the reference flow field as reported by Thangam and Speziale [13], i.e., for a solid floor. The reattachment length based on the numerical simulation was 7.25 step heights. This is only 2% longer than the

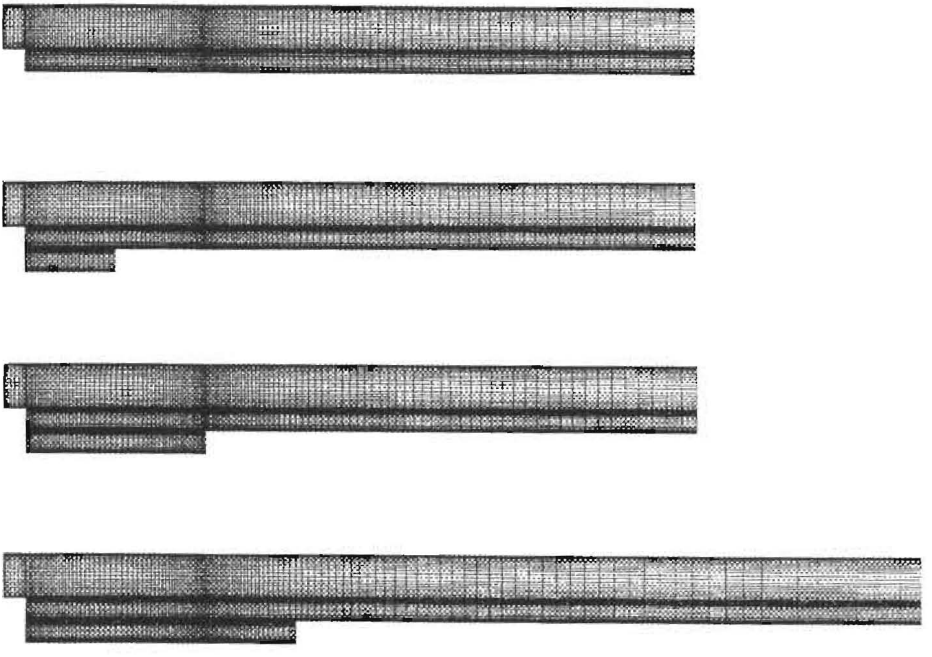

Fig. 2. Finite element mesh used for, from top: a) reference flow, b) short porous segment, c) intermediate porous segment, and d) long porous segment.

experimental value of 7.1 H [13]. The difference could be attributed to one or more of the following reasons. The current simulation is for a 2-D flow model which does not take into

account the 3-D effect of the side walls. A recent paper by Papadopoulos and Ötügen [16] shows that there is a slight variation in the reattachment location even at channel aspect ratio greater than 20. The difficulty of measuring the reattachment location experimentally as well as the dependence of the results on the measuring technique used can also lead to errors [16]. The error between the predicted and reported normalized maximum turbulent kinetic energy (TKE) was higher. The predicted value of 0.027 was about 11% less than the reported value, approximately 0.03. The effect of the 3-D structure of the experimental flow could be the cause of the higher turbulence levels. Another important issue is that the experimental results reported by Kim *et al.* [10] were based on the use of hot wire anemometer. It is well known that the use of a hot wire can alter the flow field. The effect of the addition of the porous segments reported herein will be discussed in terms of the percent change relative to the reference flow field as predicted by the code. Thus the difference between the experimental and numerical results is not expected to change the conclusions of this study. The reference flow field values used were X_r= 7.25, U_{rec} = 3.06, and TKE = 0.027.

Discussion

Figure 3 shows the percent change in the reattachment length (X_r) at different pressure loss coefficient (KP) values for the three porous segments. For the case of the short porous segment, X_p = 4, the change in X_r is small. For low KP values (< 10) the change in X_r is relatively constant (≈7%). As KP increases, the porous segment acts more like a solid wall. At KP = 10^5, the change in X_r is almost zero. At this point, the effect of the porous segment on the flow field has ended. For the medium porous segment, X_p = 8, the change in X_r is more evident. At low KP values (< 1) the flow penetrates into the porous segment and then curves up to flow over the end of the porous segment. The solid wall at the end of the porous segment acts now as forward facing step. Thus, the flow reattaches on the solid floor wall after the porous segment, i.e., X_r > 8. As the value of KP increases, the flow does not penetrate as far into the porous segment and the reattachment after the forward facing part moves closer to the downstream corner of the porous segment. At KP = 10^5, the resistance of the porous segment is so high that it acts as a solid wall and the change in X_r becomes negligible. As for the long porous segment case, X_p = 12, the flow field is significantly different than in the previous two cases. For all KP values with the exception of the highest value of 10^5, the flow reattaches inside the porous segment. The solid wall at the end of the porous segment does act as a forward facing step but the flow in the porous segment at that location is too weak to flow over the step. It is interesting that the reattachment continued to occur in the porous segment even at KP = 10^4. One should recall that the extra pressure drop is proportional to KP and to U^2 and V^2. The long porous segment seems to have diffused the flow significantly. Thus with reduced U and V, the reduction in the pressure due to KP was not as significant as in the previous two cases.

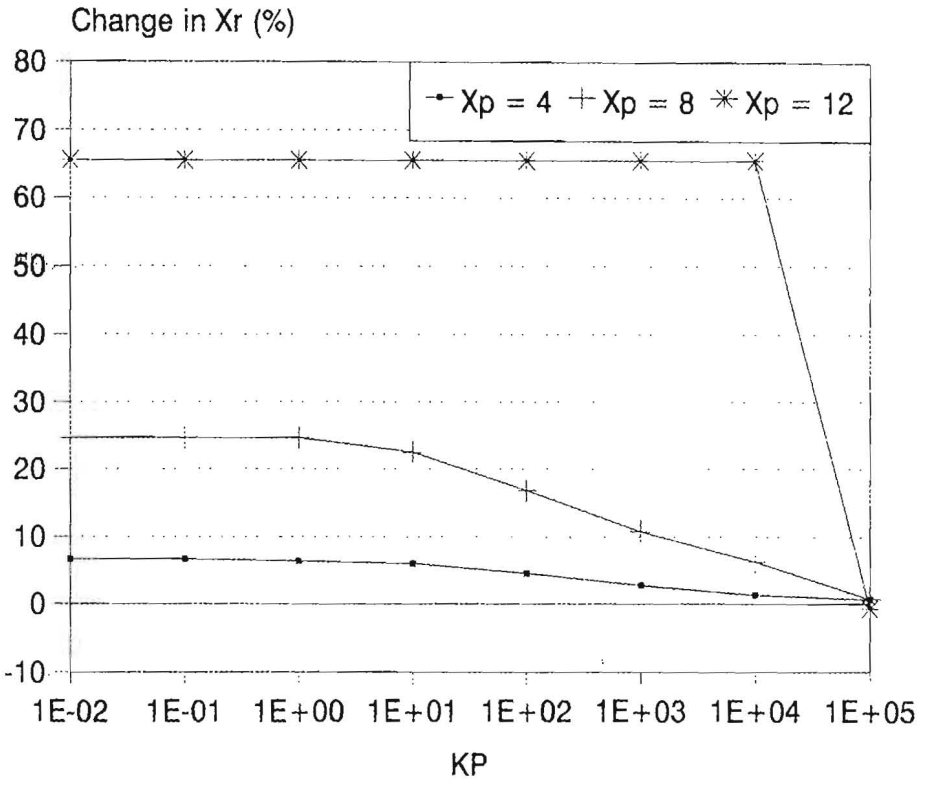

Fig. 3. Percent change in the normalized reattachment length (X_r).

Figure 4 shows the percent change in the maximum recirculation axial velocity (U_{rec}) which is defined as the maximum speed of the fluid sweeping back toward the step in the recirculation region. The value of U_{rec} is important when considering a solid fuel combustion chamber. As U_{rec} increases, the air flow will be able to erode and carry more fuel. For the case of $X_p = 4$, the change in U_{rec} with KP is small. At low KP, U_{rec} increased. This is expected as a low KP value translates into a bigger cavity in which the fluid can move. As KP increased, U_{rec} decreased and became lower than the solid wall value at KP = 10^4. At KP = 10^5, the value of U_{rec} increased but remained slightly lower than that of the reference value. The reduction in the value of U_{rec} could be attributed to the high pressure loss associated with the fluid flow through the porous segment. As the KP value increases, i.e., the porous segment starts to "solidify", a smaller fraction of lower speed fluid will pass through the porous segment resulting in reduced pressure losses. At this stage, the flow starts to recover and U_{rec} increases toward the reference value. This trend can be seen more clearly for the cases of X_p = 8 and 12. The percent change in U_{rec} ranges from a high of 35% at $X_p = 8$ and KP < 1 to a minimum of -55% at X_p = 12 and KP = 10^2. The increased length of the porous segment

coupled with the high velocity at reattachment significantly amplifies the pressure drop across the porous segment. It is interesting to note that the change in the case of $X_p = 8$ is more than that at $X_p = 12$. The minimum U_{rec} in these two cases occur at the lower KP value of 10^2 after which U_{rec} starts to recover.

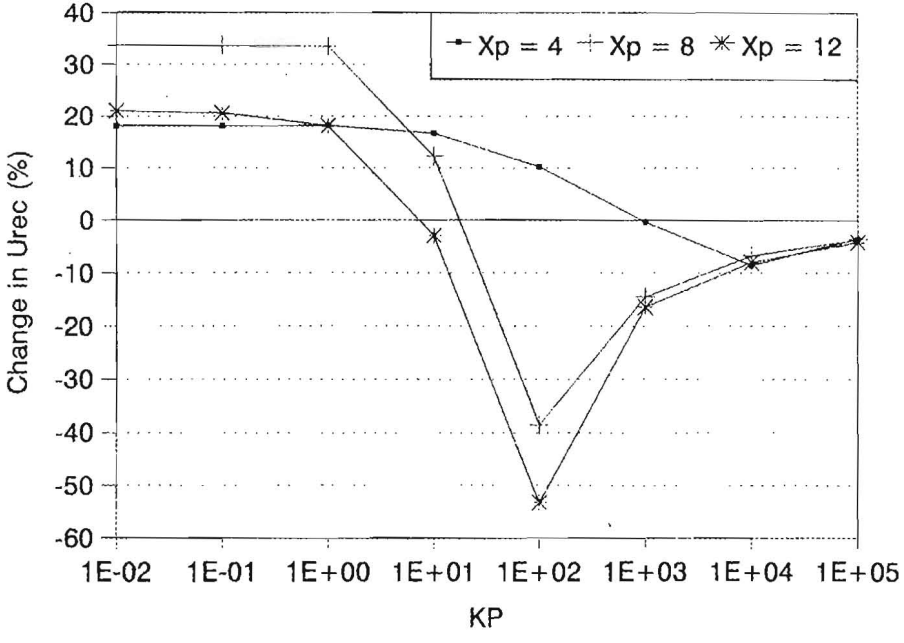

Fig. 4. Percent change in the normalized maximum axial recirculation velocity (U_{rec}).

Figure 5 shows the percent change in the normalized maximum turbulent kinetic energy (TKE). High levels of TKE are desirable in order to improve the mixing between the free stream and the fuel introduced at the base region. The mixing action is important regardless of the type of fuel used, i.e., solid, liquid, or gas. The effect of adding the short porous section, $X_p = 4$, was a slight reduction in TKE. The change in TKE is more significant in the cases of $X_p = 8$ and 12. At low KP values, the value TKE increased by approximately 9% and 17% for the cases of $X_p = 8$ and 12, respectively. A lower TKE value is desirable in cases where drag reduction is an advantage, e.g., at the base of a rocket. As the KP value is increased, TKE starts to decrease. The lowest percent change in TKE for both $X_p = 8$ and 12 cases occur at KP = 10^3, after which TKE starts to recover. At KP = 10^5, TKE has almost fully recovered to the value of the reference flow.

One might argue, with good justification, that the change in TKE is not sufficient to

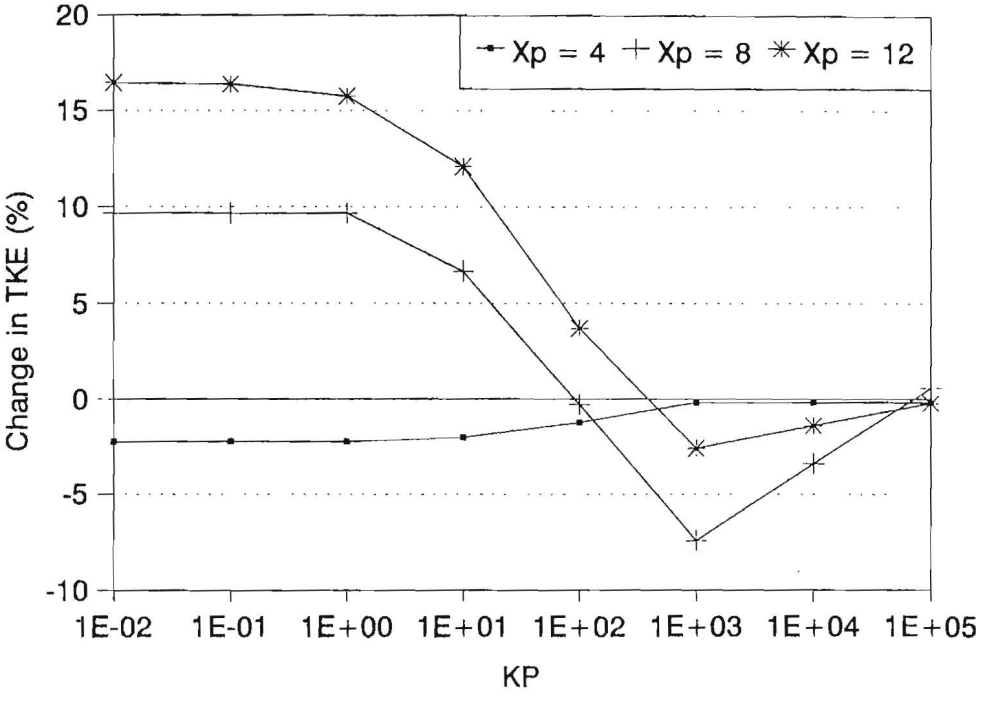

Fig. 5. Percent change in the normalized maximum turbulent kinetic energy (TKE).

describe the overall effect of the porous segments on the flow field. Figure 6 shows selected turbulent kinetic energy contours. The contours of the reference flow are also shown in the same figure for comparison. The scale is common to all contours. Figure 6.b shows the turbulence contours for the case of $X_p = 4$ and $KP = 10^{-2}$. It is clear that the change in the overall distribution of turbulent kinetic energy is small compared to that of the reference flow (Fig. 6.a). Figure 6.c shows an increase in the high turbulence regions for the case of $X_p = 8$ and $KP = 1$. The same can be seen in Fig. 6.d for the case of $X_p = 12$ and $KP = 1$. In Fig. 6.d the size of the central contour, the highest turbulent kinetic energy, is significantly larger than that in Fig. 6.c. Figure 6 seems to indicate that the change in TKE and the variation in the turbulent kinetic energy contours are closely related. Thus the information shown in Fig. 5 and the subsequent conclusions could also be generalized to most of the flow field.

Conclusions

The addition of a porous segment as part of the floor of a backward facing step configuration can be used to modify the resulting flow field. Based on the porous section

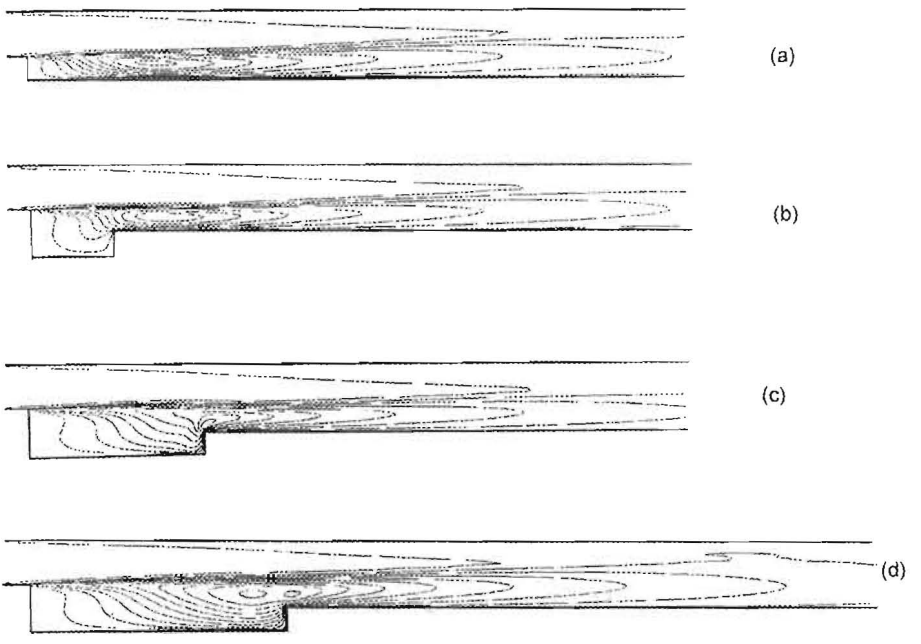

Fig. 6. Turbulent kinetic energy contours for, from top: a) reference flow, b) X p = 4 and KP=10^{-2}, c) X p =8 and KP =1, and d) X p = 12 and KP =1.

length and pressure loss coefficient, the values of X_r, U_{rec}, and TKE are all affected in different ways. A short porous segment, $X_p = 4$, results in minimal changes in X_r and TKE and a small change in U_{rec}. Thus, such a segment could be used when there is a need to introduce fuel into the base region, but without significant changes in the overall flow field. The use of longer porous segments results in more significant changes in the flow field. At the largest pressure loss coefficient used, $KP = 10^5$, all porous segments tend to act as a solid wall. The change in the overall turbulent kinetic energy distribution is closely related to the change in TKE. This significantly reduces the work required in order to study the effect of the porous segments on the overall behavior of the flow field.

References

[1] Joslin, R.D., Nicolaides, R.A., Erlebacher, G., Hussaini, M.Y. and Gunzburger, M.D. "Active Control of Boundary-layer Instabilities: Use of Sensors and Spectral Controller". *AIAA Journal*, 33, No. 8 (1995), 1521-1523.

[2] Chyu, W.J., Rimlinger, M.J. and Shih, T.I-P. "Control of Shock-wave/ Boundary-layer Interactions by Bleed". *AIAA Journal*, 33, No. 7 (1995), 1239-1247.

[3] Barter, J.W. and Dolling, D.S. "Reduction of Fluctuating Pressure Loads in Shock/Boundary-layer Interaction Using Vortex Generators". *AIAA Journal*, 33, No. 10, (1995), 1842-1849.

[4] Karl, L.D. and Fasel, H.F. "Direct Numerical Simulation of Passive Control of Three-dimensional Phenomena in Boundary-layer Transition Using Wall Heating". *Journal of Fluid Mechanics*, 264 (1994), 213-254.

[5] Garsul, I., Srinivas, S. and Batta, G. "Active Control of Vortex Breakdown over a Delta Wing". *AIAA Journal*, 33, No. 9 (1995), 1743-1745.

[6] Viswanabh, P.R. and Mukund, R. "Turbulent Drag Reduction Using Riblets on a Supercritical Airfoil at Transonic Speeds" *AIAA Journal*, 33, No. 5 (1995), 945-947.

[7] Zhang, X. "Compressible Cavity Flow Oscillation due to Shear Layer Instability and Pressure Feedback". *AIAA Journal*, 33, No. 8 (1995), 1404-1411.

[8] Hanna, R.L. "Hypersonic Shockwave/Turbulent Boundary-layer Interactions on a Porous Surface". *AIAA Journal*, 33, No. 10 (1995), 1977-1979.

[9] Gad-el-Hak, M. and Bushnell, D.M. "Separation Control: Review". *Journal of Fluids Engineering*, 113, No. 1 (1991), 5-30.

[10] Kim, J., Kline, S.J. and Johnston, J.P. "Investigation of a Reattaching Turbulent Shear Layer: Flow Over a Backward-Facing Step". *Journal of Fluids Engineering*, 102, No. 3 (1980), 302-308.

[11] Mohammadi, B. and Pironneau, O. *Analysis of the K-Epsilon Turbulence Model*. New York: John Wiley & Sons, 1993.

[12] Idelchik, I.E. *Handbook of Hydraulic Resistance*, 3rd. ed., Boca Raton CRC Press, 1994.

[13] Thangam, S. and Speziale, C.G. "Turbulent Flow Past a Backward-facing Step: A Critical Evaluation of Two-Equation Models". *AIAA Journal*, 30, No. 5 (1992), 1314-1320.

[14] Yakhot, V. and Orszag, S.A. "Renormalization Group Analysis of Turbulence: I. Basic Theory". *Journal of Scientific Computing*, 1, No. 1 (1986), 3-51.

[15] Anderson, J.D. *Computational Fluid Dynamics: The Basics with Applications*. New York: McGraw Hill, 1994.

[16] Papadopoulos, G. and Ötügen, M.V. "Separating and Reattaching Flow Structure in a Suddenly Expanding Rectangular Duct". *Journal of Fluids Engineering*, 117, No. 1(1995), 17-23.

إعادة اتصال طبقة مستعرضة مضطربة فوق عتبة خلفية ذات أرضية بمقاطع مسامية موحدة الخواص

بسام عبدالكريم أبوحجلة

قسم الهندسة الميكانيكية، جامعة العلوم و التكنولوجيا الأردنية،

ص.ب. ٣٠٣٠ ، أربد ٢٢١١٠ ، الأردن

(أستلم في ١٩٩٧/٩/٢٤م ؛ و قبل للنشر في ١٩٩٨/٢/١٦م)

ملخص البحث. تم عدديا حل عملية جريان و إعادة اتصال طبقة مستعرضة مضطربة غير قابلة للانضغاط فوق عتبة خلفية ثنائية البعد ذات عدة مقاطع مسامية موحدة الخواص باستخدام طريقة العناصر المحدودة. تم التأكد من دقة الحل العددي عن طريق مقارنة النتائج العددية مع قياسات عملية متوافرة في مجلات علمية. تم دراسة ثلاث مقاطع أرضية مسامية موحدة الخواص ذات أطوال قياسية تبلغ ٤ ، ٨ ، ١٢. تم تغيير مسامية كل مقطع علي مدي واسع عن طريق تغيير معامل خسارة الضغط. تم تقديم و مناقشة التغير في مسافة إعادة الاتصال القياسية و أكبر سرعة عكسية قياسية و أكبر طاقة حركة اضطرابية قياسية لجميع الأشكال. تبين النتائج أنه تبعا لطول و معامل خسارة الضغط للمقطع المسامي فإن أرضية مزودة بمقطع مسامي يمكن أن تحدث تغير مهم في القيم القياسية لمسافة إعادة الاتصال و أكبر سرعة عكسية و أكبر طاقة حركة اضطرابية.